JMEPEG (2017) 26:813–821
DOI: 10.1007/s11665-017-2507-z

1059-9495/$19.00

Effects of Laser Shock Processing on Fatigue Crack Growth in Ti-17 Titanium Alloy

Shuai Huang, Ying Zhu, Wei Guo, Peng Peng, Hongchao Qiao, Xungang Diao, and Paul K. Chu

(Submitted August 15, 2016; in revised form December 14, 2016; published online January 12, 2017)

The effects of laser shock processing (LSP) on the fatigue crack properties of Ti-17 titanium alloy are investigated. Surfaces on either side of a fatigue slot are subjected to LSP. The residual stress of the irradiated surface is measured by x-ray diffraction measurement and fatigue crack growth testing of the treated and untreated specimens. The fatigue fracture morphology and microstructure are examined by scanning electron microscopy and transmission electron microscopy. Proliferation and tangles of dislocations occur in the Ti-17, and the density of dislocation increases after the LSP treatment. The fine spacing of the fatigue striations indicates that LSP produces residual compressive stress on the irradiated surfaces which can delay micro-crack formation and expansion. Consequently, the fatigue propagation life of the specimen increases considerably after LSP.

Keywords failure analysis, fatigue crack growth, laser shock processing, titanium

1. Introduction

Most data about high-cycle fatigue in metals and alloys are concerned with the nominal stress required to cause failure over a given number of cycles. However, smooth or notched specimens are typically used in these tests and it is difficult to distinguish between the fatigue crack initiation life and fatigue crack propagation life. When the stress applied to a component with existing cracks reaches a critical value, crack extension failure occurs. However, in the vast majority of cases, the macro-critical crack is partially initiated by small cracks, which gradually develop under cyclic loading, a process known as crack propagation. Thus, it is important to study the propagation processes of fatigue cracks, to ensure the security of components. Various methods have been developed to measure the fatigue life associated with pre-existing flaws in materials (Ref 1).

Ti-17 titanium alloy is widely used in aircraft components such as compressor disks and fan blades owing to its high strength, superior fracture toughness, and good hardenability (Ref 2-4). However, it is becoming increasingly difficult for titanium alloys to meet the fracture property requirements of structural materials currently demanded by the aerospace industry. As a result, the application of titanium alloys has been greatly limited. Two approaches may be used to address this issue. First, a new class of titanium alloys based on the damage tolerance design concept could be developed. Second, the fracture toughness of existing titanium alloys could be optimized by controlling features of their surface microstructure. The design of a new material is a complicated and expensive process, which needs many verification experiments; however, the second approach is more cost-effective and convenient (Ref 5, 6).

Laser shock processing (LSP) is a promising surface treatment technique to improve the fatigue properties of some metals and alloys (Ref 7-9). Improved fatigue, wear and anti-corrosion properties can be attained from the compressive residual stress and grain refinement induced by LSP (Ref 10, 11). In an LSP process, a sample is irradiated by a laser pulse with a nanosecond pulse width and a high intensity, on the order of GW/cm^2. Rapid evaporation takes place on the irradiated surface as a result of the high-power laser beam (Ref 12, 13), and a plasma consisting of a partially ionized gas is formed on the irradiated surface. The irradiated surface is generally coated with an opaque over-layer, such as a black paint or metallic foil tape, to increase absorbance of laser energy and avoid overheating on the surface. A transparent overlay (tamping layer) is applied to prevent the plasma from expanding away from the surface, thereby increasing the intensity of the shock wave. Water, quartz, and glass can be used for these overlays, also known as a confining medium. Other materials used for confining media include K9 glass, Pb glass, Perspex, and silicon rubber (Ref 14, 15). As a recyclable resource, water is both convenient and cost-effective. The plasma continues to absorb laser energy and expand generating a high pressure at the sample surface. The pressure is transmitted into the materials through shock waves. When the pressure exceeds the dynamic yield strength of the materials, plastic deformation occurs in the irradiated area, which changes the microstructure and properties of the materials. In some cases, plastic deformation induced by the shock waves may result in strain hardening at the surface (Ref 16).

Most studies on laser shock processing have focused on issues such as fatigue performance, microstructure, residual stress, and the hardness variation and grain refinement mech-

Shuai Huang and **Xungang Diao**, School of Physics and Nuclear Energy Engineering, Beihang University, Beijing 100191, People's Republic of China; **Ying Zhu, Wei Guo,** and **Peng Peng**, School of Mechanical Engineering and Automation, Beihang University, Beijing 100191, People's Republic of China; **Hongchao Qiao**, Shenyang Institute of Automation, Chinese Academy of Sciences, Shenyang, Liaoning 110016, People's Republic of China; and **Paul K. Chu**, Department of Physics and Materials Science, City University of Hong Kong, Tat Chee Avenue, Kowloon, Hong Kong, People's Republic of China. Contact e-mails: pppeng@buaa.edu.cn and paul.chu@cityu.edu.hk.

Table 1 Basic material properties of Ti-17 titanium alloy

Density	4650 kg/m^3
Poisson's ratio	0.28
Elastic modulus	108 GPa
Yield stress	1075 MPa
Hardness	400 $HV_{0.2}$

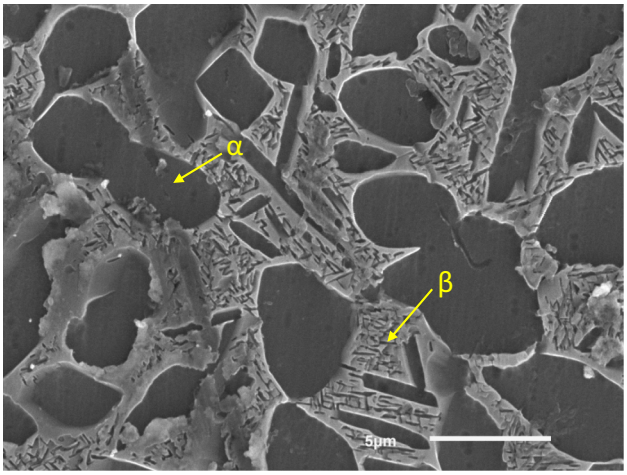

Fig. 1 Microstructures of Ti-17 titanium alloy

anisms in aluminum alloys after LSP (Ref 17-19). Huang et al. (Ref 20, 21) have shown that LSP improves the fatigue crack performance of 6061-T6 aluminum alloy. Zou et al. (Ref 22, 23) and Lin et al. (Ref 24) have also reported that the fatigue crack performance of Ti-6Al-4V is improved after LSP. Grain refinement in metals by LSP has recently become an area of research focus (Ref 25, 26). Cellard et al. (Ref 27) have reported the influence of LSP parameters on Ti-17 titanium alloy. However, there have been few studies on the crack growth life of Ti-17 titanium alloy treated by LSP. The objective of the present work is to evaluate the effects of LSP on crack growth in Ti-17 titanium alloy. The hardness and residual stress before and after LSP are determined and compared. The fracture properties and microstructure are examined by scanning electron microscopy (SEM) and transmission electron microscopy (TEM).

2. Experimental Procedures

2.1 Sample Preparation

The Ti-17 titanium alloy materials used in this study were bought from Jiaming Group Corporation (Shenzhen, China). The mechanical and physical properties of the Ti-17 titanium alloy are listed in Table 1. The samples were etched in a mixture of 90 ml of H_2O, 8 ml of HNO_3, 2 ml of HF for 15 s at room temperature. The morphologies of precipitated phases were monitored by SEM, and the microstructures of the Ti-17 titanium are shown in Fig. 1. These images show that the Ti-17 titanium alloy is an α+β two-phase alloy, which consists of fine α plates embedded in β matrix. Plates of the Ti-17 titanium alloy (10-mm thick), with the composition detailed in Table 2, were used in the experiments. The dimensions of the compact tension (CT) samples used in the fatigue crack growth (FCG)

Table 2 Chemical composition of Ti-17 titanium alloy (wt.%)

Element	Al	Cr	Zr	Sn	Mo	N	Ti
wt.%	4.5-5.5	3.5-4.5	1.6-2.4	1.6-2.4	3.5-4.5	0.013	Bal

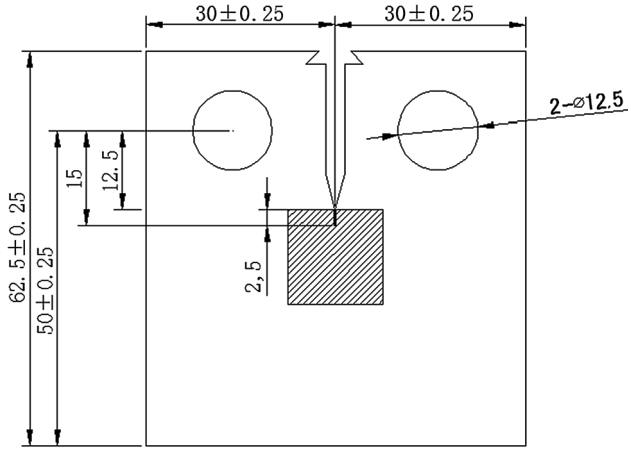

Fig. 2 Geometry of the CT specimen

test are shown in Fig. 2 according to the standard GB/T 6398-2000. The CT samples were processed with the loading axis parallel to the rolling direction and then cut by low speed one-way walk wire cut electrical discharge machining. Prior to LSP, the intended peening surfaces of specimens were ground with 1200-grit sandpaper followed by the final polishing to a surface roughness of 0.05 μm, and a fatigue pre-crack 2.5 mm long (from notch tip) was formed on each sample using a MTS-880 servo-hydraulic system at room temperature (25 °C) in air.

2.2 Laser Shock Processing

A schematic diagram and an image of the LSP equipment are shown in Fig. 3. A water layer about 2 mm thick was used as the transparent confining layer and 3-mm-wide black tape served as the ablating coating to protect the target from thermal effects. The water flow could be varied to control the thickness of water layer, which was measured with vernier calipers. In our experiment, the black tape, composed mainly of polyvinyl chloride, was bought from NITTO Co. Ltd. A Q-switched Nd:YAG laser (2-Hz repetition rate, 1064-nm wavelength, and 10-ns pulse duration) was used with a 3-mm-diameter laser shock spot, 7-J pulse energy, and 50% overlapping ratio in the LSP experiment. Prior to LSP, the samples were polished by SiC paper and a polishing cloth and then ultrasonically cleaned in alcohol.

2.3 FCG Test

The FCG tests were performed on a MTS-880 ± 100 KN fatigue test machine at room temperature (25 °C) in air. The parameters were controlled by a computer to ensure a maximum load of 5 KN, stress ratio of 0.1, and frequency of 20 Hz with a tensile sinusoidal form. The crack length was monitored by a crack opening displacement silicon chuck, and the final lives were calculated for the final instantaneous fracture length of the CT sample.

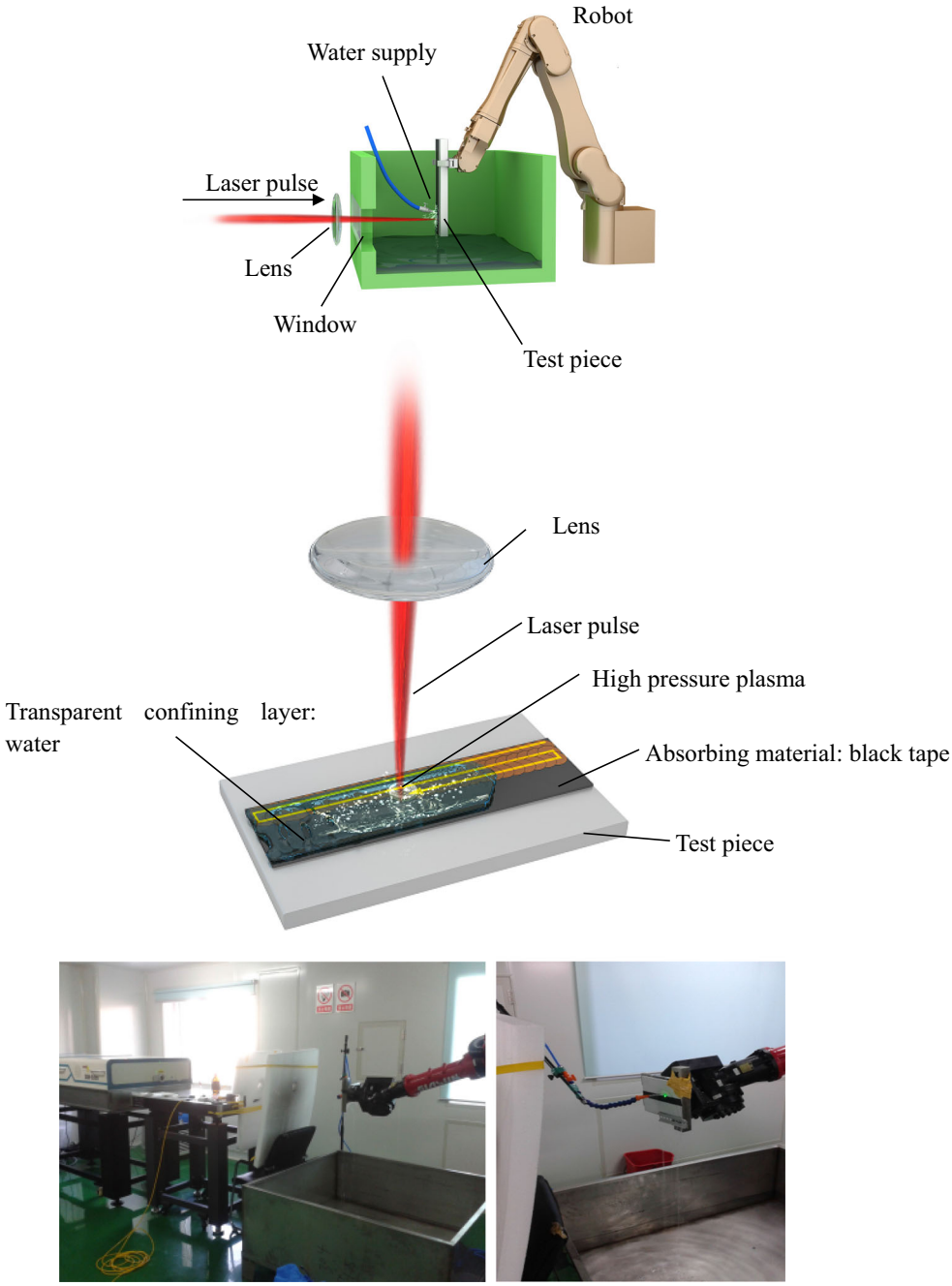

Fig. 3 Schematic diagram and image of equipment for LSP

2.4 Measurements of Residual Stress and Microstructure

After LSP, the tape was removed and the sample was cleaned with ethanol. The residual stress was determined by x-ray diffraction with the $\sin^2 \varphi$ method (x-ray diffraction tester X-350A, Handan Stress Technology Co. Ltd., China). The x-ray source was CuKα, and the x-ray beam diameter was about 1 mm. The voltage and current of the x-ray source were 26 kV and 6.0 mA, respectively. The measurements were collected at different locations across the LSP region, and the micro-hardness of the untreated and treated samples was determined on a micro-hardness tester (DHV-1000) with a 100 g load and 10 s holding time.

The specimen fracture was cut from the specimen and then cleaned ultrasonically in acetone for 20 min. SEM (JSM-6010LA, JEOL) was performed to observe the fracture morphology. The microstructural change of the samples subjected to LSP impacts was characterized by TEM. The TEM samples were prepared as follows: the substrate side of the sample was ground to a thickness less than 20 mm. A thin zone was achieved by lowering the ion milling (Gatan691) from 4.8 to 3.2 kV and decreasing the angle from 15° to 4°, over 30 min. The TEM foils at the surface were prepared by a combination of single- and twin-jet electropolishing. A JEM-2100 JEOL system with 20 kV was used for the observations.

3. Results and Discussion

3.1 Surface Morphology

The surface morphology of a single spot subjected to a laser pulse energy of 7 J is shown in Fig. 4. The circular dent after the LSP treatment is caused by plastic deformation in the region of the shock wave loading. This plastic deformation increases with increasing laser pulse energy owing to the higher shock wave pressure, which is proportional to the square root of the laser pulse energy (Ref 28). A line profile of the peened surface subjected to a 7-J pulse is shown in Fig. 4. After LSP, the treated surface exhibits a regular array of micro-dents, which can be attributed to the plastic deformations induced by successive laser irradiation at different locations (Ref 29-31). The spacing of dents depends on the shot-to-shot offset of the laser.

3.2 Micro-hardness Distribution

For most metal materials, plastic deformation enhances micro-hardness of the base material, by inducing a high density of dislocations and/or grain refinement (Ref 32). After LSP treatment, the micro-hardness distribution of the Ti-17 titanium alloy samples was measured (see Fig. 5). The depth of the gradient hardened layer was determined by analyzing the micro-hardness distribution along the cross section of the laser-peened sample. According to Chen et al. (Ref 33) and Carlsson and Larsson (Ref 34), the induced residual compressive stress can enhance the hardness of materials. The hardness along the cross section of the peened sample can be used to determine the depth of the gradient hardened layer. The micro-hardness test was used to measure the depth of the gradient hardened layer of the Ti-17 titanium alloy sample treated with LSP, as shown in Fig. 5. For the sample subjected to a laser energy of 7 J, the

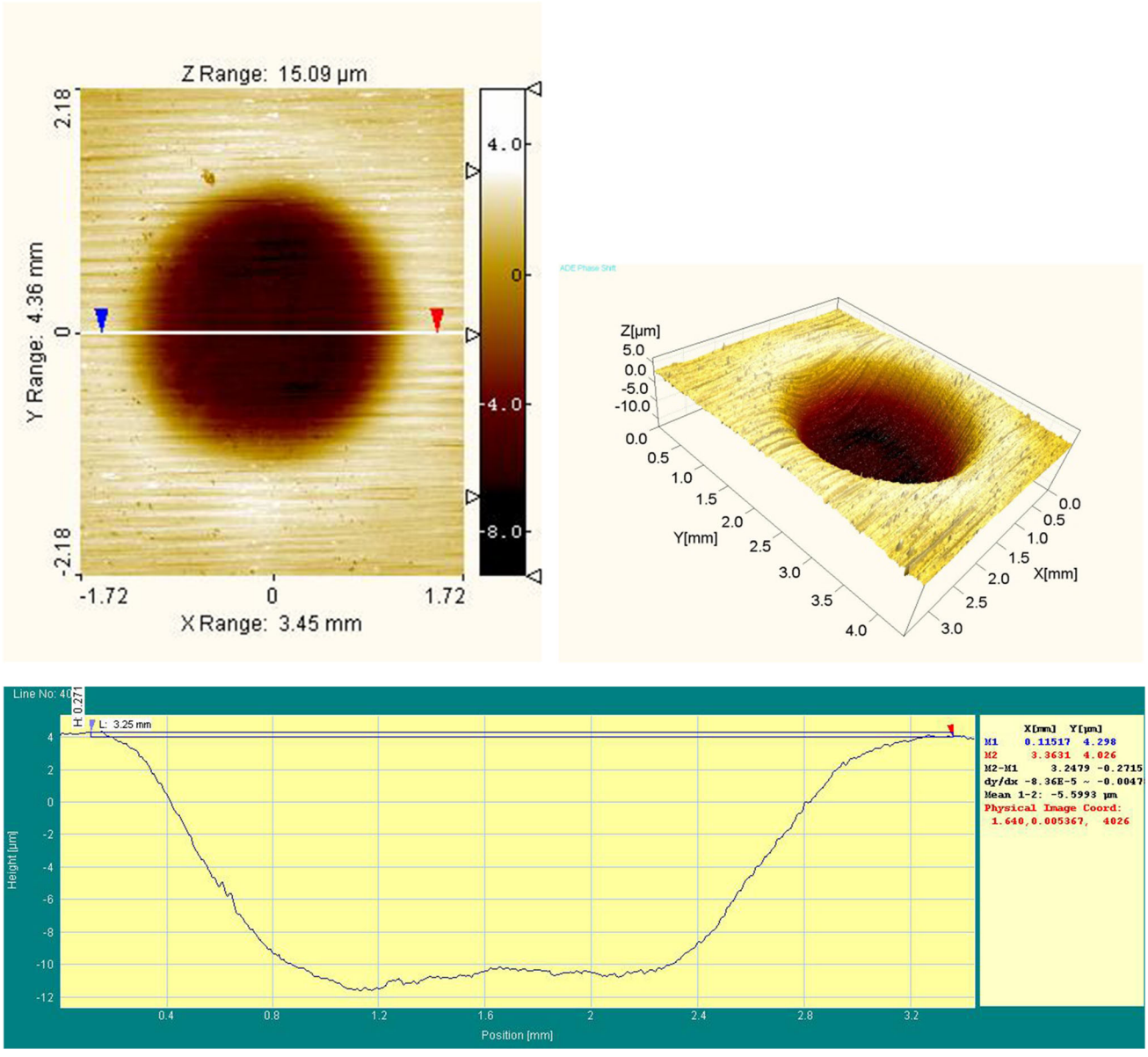

Fig. 4 Micro-dent on material surface after LSP treatment

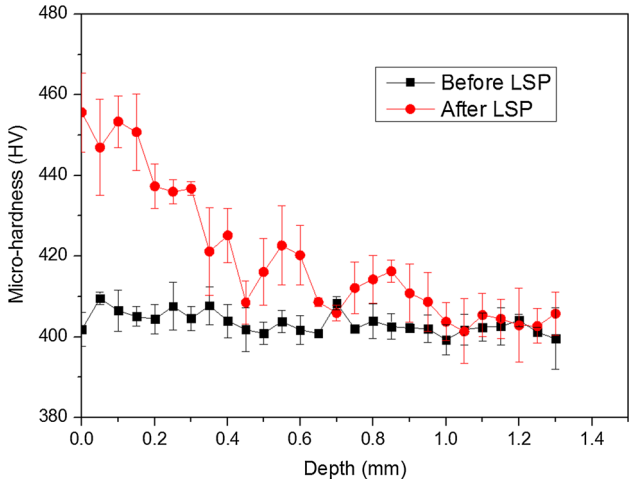

Fig. 5 Micro-hardness distribution on cross section

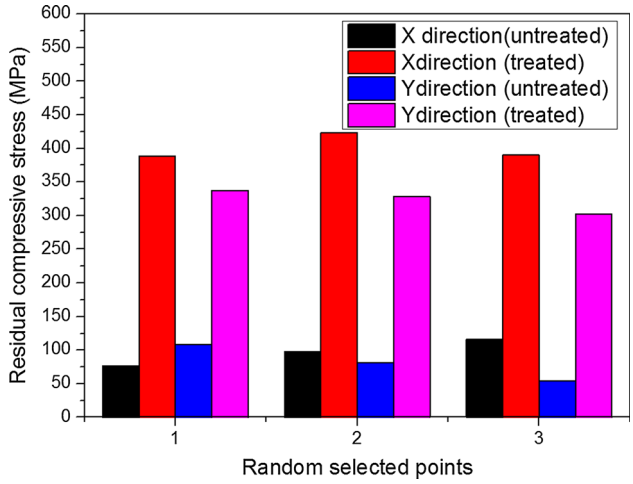

Fig. 7 Comparison of residual stress before and after LSP

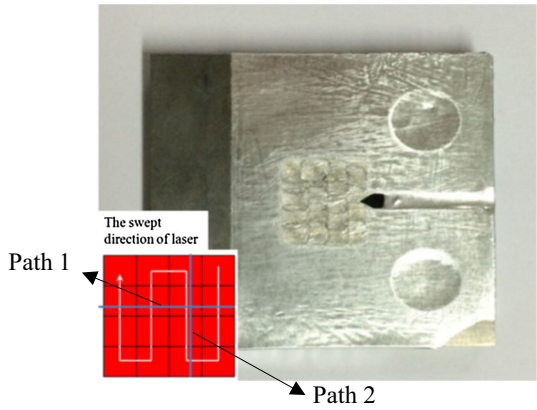

Fig. 6 Photograph of specimen after LSP

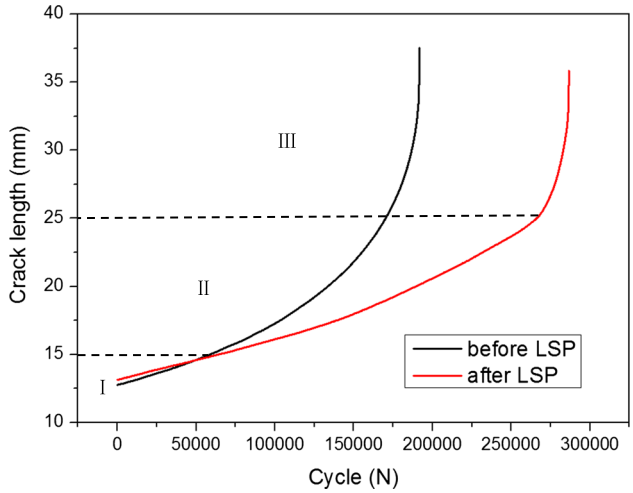

Fig. 8 Crack length vs. cycles before and after LSP

micro-hardness along the cross section increases at the surface of the gradient hardened layer and then gradually decreases to the value of the untreated region at a depth of (1.00 ± 0.05) mm, as shown in Fig. 5.

3.3 Residual Stress

The residual stress components of σ_{xx} (parallel to pulse scan direction) and σ_{yy} (perpendicular to pulse scan direction) should be considered and are reported along paths 1 and 2, respectively, as shown in Fig. 6. The residual compressive stress results of the untreated and LSP-treated samples are shown in Fig. 7. The residual stress in the two orthogonal directions exhibits a similar trend because of the similar loading conditions during LSP.

When a strong laser shock wave is applied to the surface, a permanent strain is produced. The permanent strained region is counteracted by the surrounding materials leading to compressive stress. For multiple applications of LSP, the residual stress increases with the number of laser pulses. Thus, a larger residual compressive stress is induced by LSP and this is the main factor that improves the fatigue limits and reduces the fatigue gap sensitivity (Ref 8, 18).

3.4 FCG Results

Figure 8 shows curves of the crack length a versus number of cycles N for the CT samples before and after LSP. The effective length of the initial crack is 15 mm, and the final fatigue life of the untreated sample is 191,736 cycles compared with 286,593 cycles for the treated sample. Thus, LSP increases the fatigue life of the Ti-17 titanium alloy by 49.47%. As shown in Fig. 8, when the crack length is about 15 mm, the two curves begin to separate, indicating that the crack in the LSP sample propagates slowly during this period.

According to the crack size versus elapsed cycle data (a-N), the crack growth rate d_a/d_n is calculated. The crack tip stress intensity factor range, $\Delta K = K_{\max} - K_{\min}$, is calculated from the maximum and minimum loads of the loading cycles. The fatigue crack growth data are expressed in terms of a Paris power-law expression, in which the Paris law parameters, C and m, are constants (Ref 23):

$$\frac{d_a}{d_n} = C(\Delta K)^m \qquad \text{(Eq 1)}$$

The complete curve of the FCG rate can be qualitatively divided into three sections: near-threshold, stable expansion,

and rapid expansion. Region II (Fig. 8) is the Paris region defined by a power-law relationship that corresponds to a straight line on a $\log(d_a/d_n)$ versus $\log(\Delta K)$ curve. This data reduction technique, explained in ASTM E647-08, gives the ΔK increase corresponding to regions II and III.

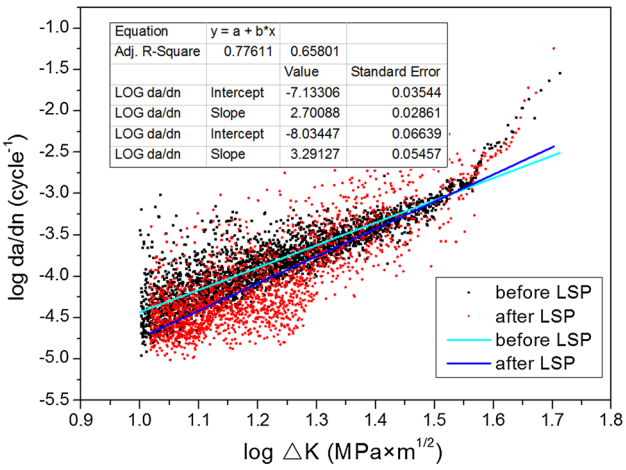

Fig. 9 Fatigue crack growth rates before and after LSP

The rate of fatigue crack growth at the near-threshold ΔK_{th} is quite slow. The large scatter in the data and influence of pre-cracking conditions make it difficult to determine ΔK_{th} as observed by Motz et al. (Ref 35). Thus, these complications hinder the ΔK_{th}-decreasing test in region I.

In region III, the crack growth rate is large and obtaining data in this unstable region is also difficult. For fatigue life prediction, region III is usually not considered because the number of cycles in this region is insignificant compared with the total fatigue life. Here, regions I and III are not considered.

The ΔK-increasing test is performed, and the fatigue crack growth rate or d_a/d_n is obtained from the slope of the a-N curve under displacement-controlled conditions.

Before LSP, the Paris formulation is:

$$\frac{d_a}{d_n} = 7.98 \times 10^{-4} \times (\Delta K)^{2.70088}$$

After LSP, the Paris formulation is

$$\frac{d_a}{d_n} = 3.24 \times 10^{-4} \times (\Delta K)^{3.29127}$$

The Paris formula was fitted to the relationship of the curves, and changes in the constant values C and m are detailed in Fig. 9. Similar results have been reported in previous crack

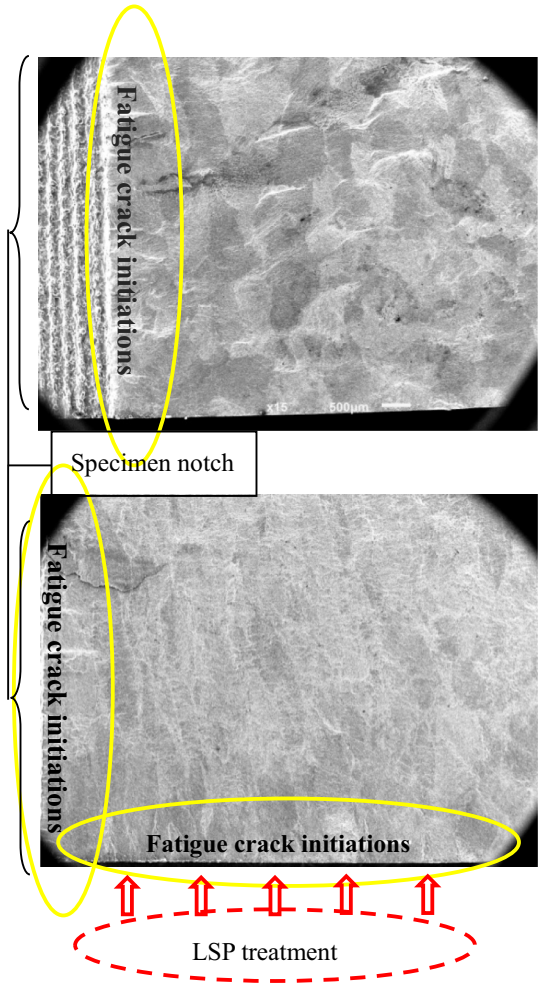

Fig. 10 Morphology of fatigue crack origins

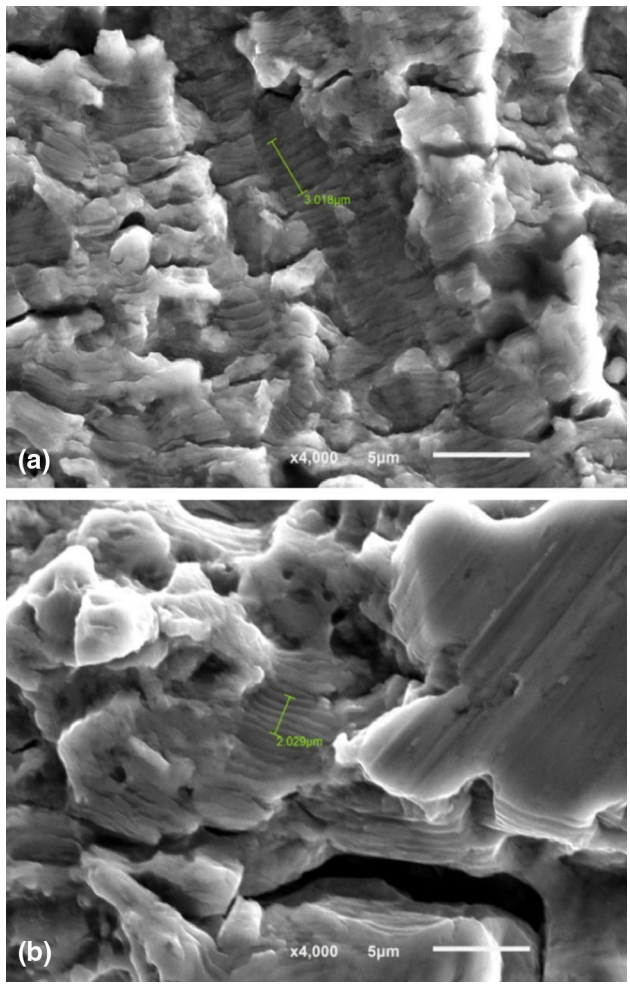

Fig. 11 Micromorphology of the fatigue striations in the stable crack growth zone: (a) untreated and (b) treated

propagation studies (Ref 36, 37). LSP reduces the FCG rate compared with untreated samples as indicated by the decline in the d_a/d_n and ΔK curves. The reduction of d_a/d_n is clear in the initial period of FCG. However, when ΔK increases to large values in the final period of FCG, the FCG rates of the samples before and after LSP are almost the same.

The improvement in the FCG resistance induced by LSP can be separated into a relatively large increase in the initial FCG stage (Stage II in Fig. 8) and a slight increase in the final FCG stage (Stage III in Fig. 8). In the initial FCG stage, the residual compressive stress induced by LSP causes crack closure and reduces the effective driving force, which leads to a reduction of ΔK and d_a/d_n (Ref 38). However, the residual compressive stress relaxes with increasing of crack length and the FCG rate decreases more slowly (Ref 18). In the LSP samples, the crack arrest effects in the final FCG stage are limited because the crack driving force is much larger than the resistance induced by the residual compressive stress.

3.5 Fracture Morphology

The fracture morphology of specimens with and without the LSP treatment is examined by SEM. In Fig. 10, the locations of fatigue crack initiation (FCI) are shown on the fracture surface under different conditions (as indicated by yellow circles). A FCI exists at each slot entrance on the untreated surface, whereas there are two crack initiations on the treated surface. After LSP, the fracture appears flatter owing to compressive stress generated in the surface layer, which counters the tensile stress from transforming to compressive stress and increases the resistance to fatigue crack nucleation.

Figure 11 shows the micromorphology of the stable crack growth zone of samples treated under different conditions. The microstructure occurred at the same place on the fracture surface 5 mm away from the edge of the slot. Clear fatigue striations are observed from the fracture surface as wavy stripes. These parallel fatigue striations are characteristic of a fatigue fracture that occurs in the direction perpendicular to that of the crack growth. From Fig. 11(a), the fatigue striation spacing is determined as 0.6-0.7 μm/cycle for unLSP treated sample, while the average value of LSP treated is 0.4-0.5 μm/cycle as observed in Fig. 11(b). The spacing between the fatigue striations shows the distance of crack growth per cycle. Therefore, the crack growth rate of the untreated sample is faster than that of the LSP-treated sample in line with the FCG results.

3.6 Microstructures

Figure 12 shows TEM images of the Ti-17 titanium alloy before and after LSP. The microstructure is refined after LSP,

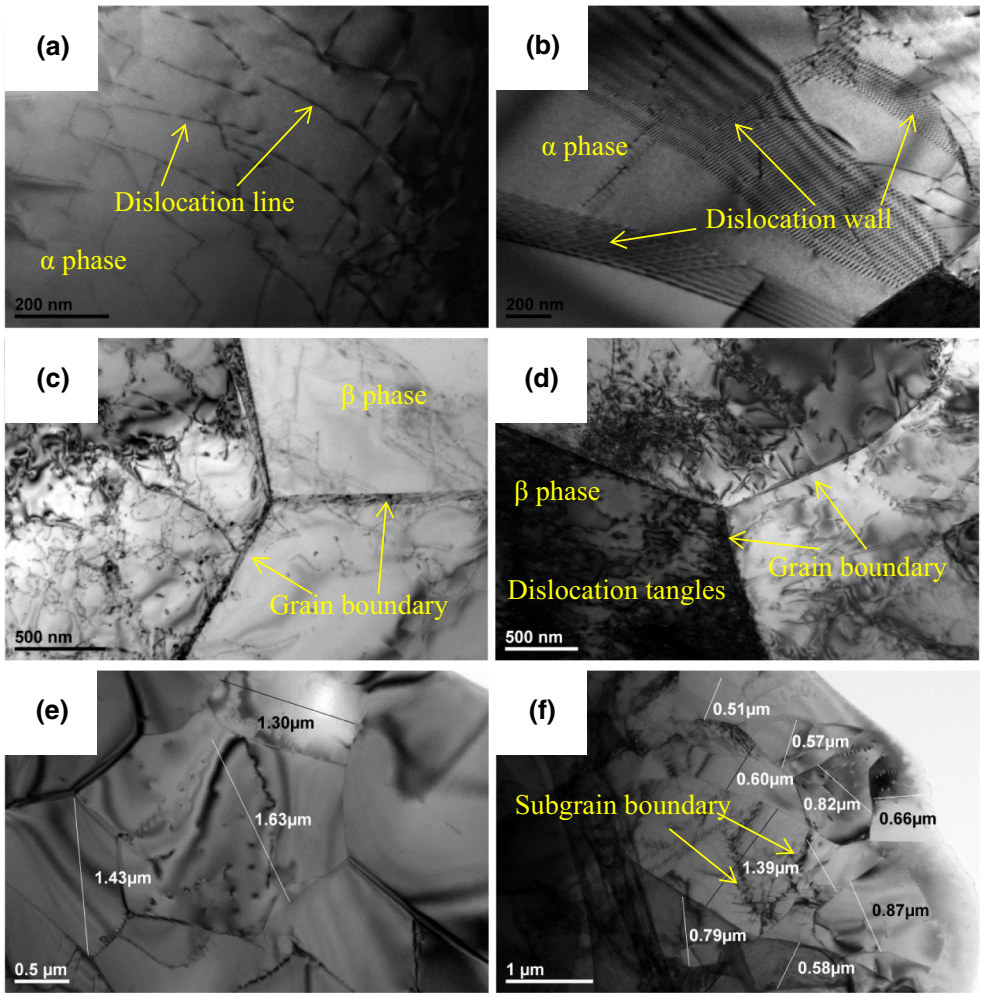

Fig. 12 TEM images of the Ti-17 titanium alloy surface: (a) density of dislocations (untreated); (b) density of dislocations (treated); (c) sub-grain (untreated); (d) sub-grain (treated); (e) nanocrystalline (untreated); (f) nanocrystalline (treated)

and the fatigue performance is improved. High-density dislocations can be seen on the irradiated surface. These high-density dislocations improve the yield strength of the titanium alloy. The existence of many dislocations and their movement can prevent initiation and propagation of fatigue cracks so that fatigue resistance is improved (Ref 39).

As shown in Fig. 12(a), deformed twins aligning in one direction are observed in the base material; however, no twinning intersections are observed. A high density of twins is formed after LSP, as shown in Fig. 12(b). Typical microstructures including twins and obvious dislocation movements are observed in an α phase. Figure 12(c) shows a typical TEM image of the β phase of the base material. Many dislocation lines can be observed in coarse grains, and some dislocation lines disappear near grain boundaries. In Fig. 12(d), dislocation multiplication is observed in the grains treated by LSP and their high density means that the dislocations tangle with each other. At high densities, the dislocations will annihilate and rearrange near tangles and walls to reduce the total energy of the grain system. These dislocation tangles and dislocation walls further develop into low-angle sub-grain boundaries that result in refinement of the coarse grains (Ref 40). The nanostructure of the titanium alloy surface after LSP is shown in Fig. 12(f). The uncertain orientation relationship between neighboring sub-grains in the nanostructure results in a sliding channel length lower than the grain length scale. Consequently, crack propagation is twisted and the strength of the materials is improved.

In the materials subjected to the laser-induced shock wave, dislocations and plastic deformation are produced by dislocation slip and shock wave reflection and refraction at grain boundaries. The shock wave induces various effects on the grains resulting in dislocations after complex slip events, agglomeration and annihilation to form new grain boundaries, smaller grains, and a higher density of dislocations. In addition, there is the Hall-Petch relationship between the rupture stress and grain diameter:

$$\sigma = \sigma_0 + Kd^{-1/2} \quad \text{(Eq 2)}$$

where σ is the rupture stress, σ_0 is the basic rupture stress, K is a constant related to the materials, and d is the grain diameter. According to Eq 2, the rupture stress is inversely proportional to the grain diameter. After LSP, the average diameter of grains is smaller than that of the original materials. Thus, LSP improves the rupture stress, and the samples subjected to LSP require more energy to fracture (Ref 41).

A grain refinement mechanism during LSP is proposed. The results show that ultra-high strain and strain rates are involved in the formation of dislocation lines. The accumulation of these features contributes to the formation of complex random structures such as dislocation tangles, dense dislocation walls, and dislocation cells. Increases in strain result in sub-grain formation through dislocation annihilation and formation of multiple shear bands, which leads to an ultra-fine nanograin structure (Ref 42).

4. Conclusion

LSP is an effective surface treatment technique to retard the propagation of fatigue cracks and improve the fatigue life of Ti-17 titanium alloy. Our results reveal that multiple LSP treatments have a beneficial effect on the residual stress in the superficial layers. The crack propagation rate slows because of the superficial residual compressive stress induced by LSP. After the laser treatment, the density of dislocations increases and the grain size decreases, consequently prolonging the fatigue life of the materials.

Acknowledgments

This work was supported by International Science and Technology Cooperation Program of China (Grant No. 2013DFR50590), National Natural Science Foundation of China (No. 51501219), Natural Science Foundation of Liaoning Province (No. 2015020115), and City University of Hong Kong Applied Research Grant (ARG) No. 9667104.

References

1. W.F. Smith and J. Hashemi, *Foundations of Materials Science and Engineering*, 5th ed., McGraw-Hill, New York, 2011
2. K.-X. Wang, W.-D. Zeng, and Y.-Q. Zhao, Prediction of Dynamic Globularization of Ti-17 Titanium Alloy with Initial Microstructure During Hot Compression, *Mater. Sci. Eng. A*, 2010, **527**, p 6193–6199
3. H. Li, C. Zhang, H.-B. Liu, and M.-Q. Li, Bonding Interface Characteristic and Shear Strength of Diffusion Bonded Ti-17 Titanium Alloy, *Trans. Nonferrous Met. Soc. China*, 2015, **25**, p 80–87
4. H. Li, M.Q. Li, T. Han, and H.B. Liu, The Deformation Behavior of Isothermally Compressed Ti-17 Titanium Alloy in α+β field, *Mater. Sci. Eng. A*, 2012, **546**, p 40–45
5. X. Shi, W. Zeng, and Q. Zhao, The Effects of Lamellar Features on the Fracture Toughness of Ti-17 Titanium Alloy, *Mater. Sci. Eng. A*, 2015, **636**, p 543–550
6. A. Ebach-Stahl, C. Eilers, N. Laska, and R. Braun, Cyclic Oxidation Behaviour of the Titanium Alloys Ti-6242 and Ti-17 with Ti-Al-Cr-Y Coatings at 600 and 700 °C in Air, *Surf. Coat. Technol.*, 2013, **223**, p 24–31
7. J.Z. Zhou, S. Huang, and L.D. Zou, Effects of Laser Peening on Residual Stresses and Fatigue Crack Growth Properties of Ti-6Al-4V Titanium Alloy, *Opt. Lasers Eng.*, 2014, **52**, p 189–194
8. X.D. Ren, Q.B. Zhan, and H.M. Yang, The Effects of Residual Stress on Fatigue Behavior and Crack Propagation from Laser Shock Processing-Worked Hole, *Mater. Des.*, 2013, **44**, p 149–154
9. A. Chahardehi, F.P. Brennan, and A. Steuwer, The Effect of Residual Stresses Arising from Laser Shock Peening on Fatigue Crack Growth, *Eng. Fract. Mech.*, 2010, **77**, p 2033–2039
10. D. Schnubel, M. Horstmann, and V. Ventzke, Retardation of Fatigue Crack Growth in Aircraft Aluminum Alloys via Laser Heating—Experiment Proof of Concept, *Mater. Sci. Eng. A*, 2012, **546**, p 8–14
11. C. Rubio-Gonzalez, C. Felix-Martinez, and G. Gomez-Rosas, Effects of Laser Shock Processing on Fatigue Crack Growth of Duplex Stainless Steel, *Mater. Sci. Eng. A*, 2011, **528**, p 914–919
12. S. Zabeen, M. Preuss, and P.J. Withers, Evolution of a Laser Shock Peened Residual Stress Field Locally with Foreign Object Damage and Subsequent Fatigue Crack Growth, *Acta Mater.*, 2015, **83**, p 216–226
13. A.K. Gujba and M. Medraj, Laser Peening Process and Its Impact on Materials Properties in Comparison with Shot Peening and Ultrasonic Impact Peening, *Materials*, 2014, **7**, p 7925–7974
14. X. Hong, S. Wang, D. Guo, H. Wu, J. Wang, Y. Dai, X. Xia, and Y. Xie, Confining Medium and Absorptive Overlay: Their Effects on a Laser-Induced Shock Wave, *Opt. Lasers Eng.*, 1989, **29**, p 447–455
15. A. Kruusing, Underwater and Water-Assisted Laser Processing: Part 1—General Features, Steam Cleaning and Shock Processing, *Opt. Lasers Eng.*, 2004, **41**, p 307–327
16. X. Zhang, L. Chen, and Yu Xiaoliu, Effect of Laser Shock Processing on Fatigue Life of Fastener Hole, *Trans. Nonferrous Met. Soc. China*, 2014, **24**, p 969–974
17. X.Q. Zhang, H. Li, and X.L. Yu, Investigation on Effect of Laser Shock Processing on Fatigue Crack Initiation and Its Growth in Aluminum Alloy Plate, *Mater. Des.*, 2015, **65**, p 425–431

18. C. Correa, L. Ruiz de Lara, and M. Diaz, Influence of Pulse Sequence and Edge Material Effect on Fatigue Life of Al2024-T351 Specimens Treated By Laser Shock Processing, *Int. J. Fatigue*, 2015, **70**, p 196–204
19. F. Qi, P. Staron, and V. Ventzke, Effect of Local Laser Surfacing on the Fatigue Crack Propagation Rate of Al-Alloy 6065 and Its Laser Beam Weld, *Proc. Mater. Sci.*, 2014, **3**, p 1834–1840
20. S. Huang, J.Z. Zhou, and J. Sheng, Effects of Laser Energy on Fatigue Crack Growth Properties of 6061-T6 Aluminum Alloy Subjected to Multiple Laser Peening, *Eng. Fract. Mech.*, 2013, **99**, p 87–100
21. S. Huang, J.Z. Zhou, and J. Sheng, Effects of Laser Shock Peening with Different Coverage Areas on Fatigue Crack Growth Properties of 6061-T6 Aluminum Alloy, *Int. J. Fatigue*, 2013, **47**, p 292–299
22. C.A.O. Ziwen, X.U. Haiying, and Z.O.U. Shikun, Investigation of Surface Integrity on TC17 Titanium Alloy Treated by Square-Spot Laser Shock Peening, *Chin. J. Aeronaut.*, 2012, **25**, p 650–656
23. S. Zou, S. Gong, and E. Guo, Surface Profile and Microstructure of Laser Peened Ti-6Al-4V, *Rare Met.*, 2012, **31**, p 430–433
24. B. Lin, C. Lupton, and S. Spanrad, Fatigue Crack Growth in Laser Shock Peened Ti-6Al-4V Aerofoil Specimens Due to Foreign Object Damage, *Int. J. Fatigue*, 2014, **59**, p 23–33
25. C. Rubio-Gonzalez, J.L. Ocana, and G. Gomez-Rosas, Effect of Laser Shock Processing on Fatigue Crack Growth and Fracture Toughness of 6061-T6 Aluminum Alloy, *Mater. Eng. A*, 2004, **386**, p 291–295
26. S. Kashef, A. Asgari, and T.B. Hilditch, Fatigue Crack Growth Behavior of Titanium Foams for Medical Applications, *Mater. Sci. Eng. A*, 2011, **528**, p 1602–1607
27. C. Cellard, D. Retraint, M. Francois, E. Rouhaud, and D. Le Saunier, Laser Shock Peening of Ti-17 Titanium Alloy: Influence of Process Parameters, *Mater. Sci. Eng. A*, 2012, **532**, p 362–372
28. C.H. Yang, P.D. Hougson, Q.C. Liu et al., Geometrical Effects on Residual Stresses in 7050-T7451 Aluminum Alloy Rods Subject to Laser Shock Processing, *J. Mater. Process. Technol.*, 2008, **201**, p 303–309
29. X.Q. Zhang, H. Li, X.L. Yu et al., Investigation on Effect of Laser Shock Processing on Fatigue Crack Initiation and Its Growth in Aluminum Alloy Plate, *Mater. Des.*, 2015, **65**, p 425–431
30. A. Chahardehi, F.P. Brennan, and A. Steuwer, The Effect of Residual Stresses Arising from LSP on Fatigue Crack Growth, *Eng. Fract. Mech.*, 2010, **77**, p 2033–2039
31. S. Huang, J.Z. Zhou, J. Sheng, K.Y. Luo et al., Effects of Laser Peening with Different Coverage Areas on Fatigue Crack Growth Properties of 6061-T6 Aluminum Alloy, *Int. J. Fatigue*, 2013, **47**, p 292–299
32. J.Z. Lu, K.Y. Luo, Y.K. Zhang et al., Grain Refinement Mechanism of Multiple Laser Shock Processing Impacts on ANSI, 304 Stainless Steel, *Acta Mater.*, 2010, **58**, p 5354–5362
33. X. Chen, J. Yan, and A.M. Karlsson, On the Determination of Residual Stress and Mechanical Properties by Indentation, *Mater. Sci. Eng. A*, 2006, **416**, p 139–149
34. S. Carlsson and P.L. Larsson, On the Determination of Residual Stress and Strain Fields by Sharp Indentation Testing. Part I: Theoretical and Numerical Analysis, *Acta Mater.*, 2001, **49**, p 2179–2191
35. C. Motz, O. Friedl, and R. Pippan, Fatigue Crack Propagation in Cellular Metals, *Int. J. Fatigue*, 2005, **27**, p 1571–1581
36. O. Hatamleh, A Comprehensive Investigation on the Effects of Laser and Shot Peening on Fatigue Crack Growth in Friction Stir Welded AA 2195 Joints, *Int. J. Fatigue*, 2009, **31**, p 974–988
37. G. Bussu and P.E. Irving, The Role of Residual Stress and Heat Affected Zone Properties on Fatigue Crack Propagation in Friction Stir Welded 2024-T351 Aluminium Joints, *Int. J. Fatigue*, 2003, **25**, p 77–88
38. E. Maawad, Y. Sano, L. Wagner, and H.C. Brokmeier, Investigation of Laser Shock Peening on Residual Stress and Fatigue Performance of Titanium Alloys, *Mater. Sci. Eng. A*, 2012, **36**, p 82–91
39. P. Li, S. Huang, and X. Haifeng, Numerical Simulation and Experiments of Titanium Alloy Engine Blades Based on Laser Shock Processing, *Aerosp. Sci. Technol.*, 2015, **40**, p 164–170
40. J.Z. Lu, K.Y. Luo, and Y.K. Zhang, Grain Refinement of LY2 Aluminum Alloy Induced by Ultra-High Plastic Strain During Multiple Laser Shock Processing Impacts, *Acta Mater.*, 2010, **58**, p 3984–3994
41. H. Li, Y. Liu, and M. Li, The Gradient Crystalline Structure and Microhardness in the Treated Layer of TC17 Via High Energy Shot Peening, *Appl. Surf. Sci.*, 2015, **357**, p 197–203
42. U. Trdan, M. Skarba, and J. Grum, Laser Shock Peening Effect on the Dislocation Transitions and Grain Refinement of Al-Mg-Si Alloy, *Mater. Charact.*, 2014, **97**, p 57–68